**Supplemental item titles**

**Supplemental Figure 1 (related to all Figures):** Number of recorded, stained, and registered interneurons in each mouse for each subtype. Description of the immuno-based identification strategy.

**Supplemental Figure 2 (related to Figure 2):** Run-start and run-stop dynamics in the random foraging task, and distribution of velocity-correlation as a function of depth of the cell body in the tissue.

**Supplemental Figure 3 (related to Figure 2):** Processing flowchart and deep learning architecture of the machine-learning based decoding approach.

**Supplemental Figure 4 (related to Figure 3):** Average responses during sharp-wave ripple events and depth distributions.

**Supplemental Figure 5 (related to Figure 4):** Quantification and analysis of spatially selective interneurons with negative place fields.

**Supplemental Figure 6 (related to Figure 4 and 5):** Stability of tuning curves at three time point: within-session, 1h, and 24h apart.

**Supplemental Figure 7 (related to Figure 6):** Quantification of learning-related activity dynamics in all identified subtypes, and multivariate regression model to focus on distinct predictors of activity.

**A**

| Mouse ID | Immunostaining strategy | in vivo ROI | found in confocal | subtype assigned | PVBC | SomC | BiC | AAC | CCKC | IvC NGFC | PVBC AAC |
|---|---|---|---|---|---|---|---|---|---|---|---|
| TG14 | **1**: PV, SOM, NPY, SATB1, **2**: CCK | 247 | 206 | 158 | 40 | 49 | 31 | 20 | 5 | 13 | 0 |
| TG16 | **1**: CCK, SOM, NPY, **2**: PV, SATB1 | 245 | 165 | 86 | 1 | 19 | 11 | 6 | 8 | 17 | 24 |
| TG17 | **1**: CCK, SOM, NPY, **2**: PV, SATB1 | 248 | 121 | 66 | 10 | 4 | 7 | 4 | 0 | 17 | 24 |
| TG18 | **1**: CCK, SOM, NPY, **2**: PV, SATB1 | 223 | 199 | 135 | 45 | 30 | 13 | 8 | 6 | 33 | 0 |
| TG19 | **1**: CCK, SOM, NPY, **2**: PV, SATB1 | 231 | 84 | 75 | 25 | 10 | 3 | 9 | 15 | 13 | 0 |
| BV90 | **1**: CCK, SOM, NPY, **2**: PV, SATB1 | 267 | 213 | 138 | 9 | 35 | 25 | 8 | 5 | 8 | 48 |
| TG300 | **1**: CCK, SOM, NPY, **2**: PV, SATB1 | 245 | 226 | 145 | 15 | 53 | 11 | 9 | 1 | 12 | 44 |
| TG302 | **1**: CCK, SOM, NPY, **2**: PV, SATB1 | 231 | 211 | 126 | 2 | 46 | 8 | 4 | 9 | 12 | 45 |
| TG310 | **1**: CCK, SOM, NPY, **2**: PV, SATB1 | 297 | 254 | 130 | 10 | 39 | 5 | 3 | 13 | 21 | 39 |
| TG325 | **1**: PV, SOM, SATB1, **2**: CCK, NPY | 240 | 227 | 132 | 23 | 34 | 20 | 30 | 4 | 20 | 1 |
| TG326 | **1**: PV, SOM, SATB1, **2**: CCK, NPY | 240 | 172 | 101 | 33 | 22 | 15 | 15 | 1 | 13 | 2 |
| TG327 | **1**: PV, SOM, SATB1, **2**: CCK, NPY | 240 | 216 | 113 | 32 | 37 | 14 | 22 | 3 | 2 | 3 |

| | a-CCK | a-SOM | a-NPY | a-PV | a-SATB1 |
|---|---|---|---|---|---|
| CCKC | + | - | +/- | - | +/- |
| SomC | - | + | +/- | - | +/- |
| PVBC | - | - | - | + | + |
| AAC | - | - | - | + | - |
| BiC | - | + | + | + | + |
| IvC/NGFC | - | - | + | - | +/- |

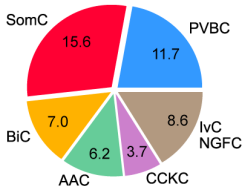


**B**

| Mouse ID | Immunostaining strategy | in vivo ROI | found in confocal | subtype assigned | PV+ | SomC | BiC | IvC NGFC | ISI1 | VIP+/CR- | ISI3 |
|---|---|---|---|---|---|---|---|---|---|---|---|
| TG276 | **1**: PV, SOM, VIP, **2**: NPY, CR | 240 | 188 | 96 | 48 | 6 | 18 | 8 | 2 | 6 | 8 |
| BV106 | **1**: PV, SOM, VIP, **2**: NPY, CR | 244 | 221 | 138 | 74 | 26 | 12 | 7 | 6 | 6 | 7 |
| BV107 | **1**: PV, SOM, VIP, **2**: NPY, CR | 234 | 213 | 118 | 70 | 30 | 2 | 3 | 2 | 7 | 4 |
| BV109 | **1**: PV, SOM, VIP, **2**: NPY, CR | 246 | 213 | 148 | 59 | 67 | 11 | 9 | 0 | 2 | 0 |

| | a-PV | a-SOM | a-NPY | a-VIP | a-CR |
|---|---|---|---|---|---|
| PV+ | + | - | + | - | - |
| SomC | - | + | +/- | - | - |
| BiC | + | + | - | - | - |
| IvC/NGFC | - | - | + | - | - |
| ISI1 | - | - | - | - | + |
| VIP+/CR- | - | - | - | + | - |
| ISI3 | - | - | - | + | + |

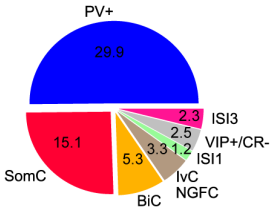


**C**

VIP-Cre mice

| Mouse ID | Immuno.strategy | in vivo ROI | found in confocal | subtype assigned | ISI3 | VIP+/CCK+ | VIP+/M2R+ | ISI2 |
|---|---|---|---|---|---|---|---|---|
| TG338 | **1**: CCK, CR, M2R | 110 | 100 | 31 | 11 | 6 | 1 | 13 |
| TG339 | **1**: CCK, CR, M2R | 126 | 114 | 38 | 21 | 5 | 1 | 11 |
| TG340 | **1**: CCK, CR, M2R | 150 | 123 | 44 | 27 | 7 | 2 | 8 |

| | a-CR | a-M2R | a-CCK |
|---|---|---|---|
| ISI2 | - | - | - |
| ISI3 | + | - | - |
| VIP+/M2R+ | - | + | - |
| VIP+/CCK+ | - | - | + |

## Figure S1 - Molecular characteristics of interneuron subtypes and breakdown of imaged cells by subtype (related to all Figures)

**A**.Top: Overview of the data analyzed in Figures 1-6. Each row includes the antigens stained for in that mouse, the number of imaged cells, the number of cells registered in the confocal images, the number of cells assigned an interneuron subtype, and the breakdown by subtype. In cases where SATB1 immunostaining was unclear, cells were assigned a general (PVBC/AAC) subtype and excluded from analysis. Bottom left: Overview of the rules used to assign interneurons to a subtype based on immunohistochemistry (see Methods). Bottom right: Percentage of registered cells belonging to each subtype. The most quantitative anatomical characterization of rodent CA1 inhibitory circuits performed to date has produced the following estimates for the numbers of each interneuron subtype (as a percentage of the total CA1 interneuron population): PVBC: 14.4%, SomC: 9.3%, BiC: 5.7%, AAC: 3.8%, CCKC: 13.9%, IvC/NGFC: 32.2% (Bezaire and Soltesz, 2013). The ratio of subtypes we identify is close to these numbers, with the largest differences in the CCKC and IvC/NGFC subtypes. These cells tend to have smaller soma diameter (Capogna, 2011; Armstrong, Krook-Magnuson and Soltesz, 2012; Overstreet-Wadiche and McBain, 2015) and exist in large numbers in the more superficial layers of CA1, making them more difficult to sample during in vivo imaging.
**B**.Top: Overview of the data analyzed in VGAT-Cre mice in Figure 7. Each row of the table includes the same information as above. Bottom left: Overview of the rules used to assign interneurons to a subtype. Bottom Right: Percentage of registered cells belonging to each subtype.
**C**.Bottom left: Overview of the data analyzed in VIP-Cre mice in Figure 7. Bottom right: Overview of the rules used to assign interneurons to a subtype.

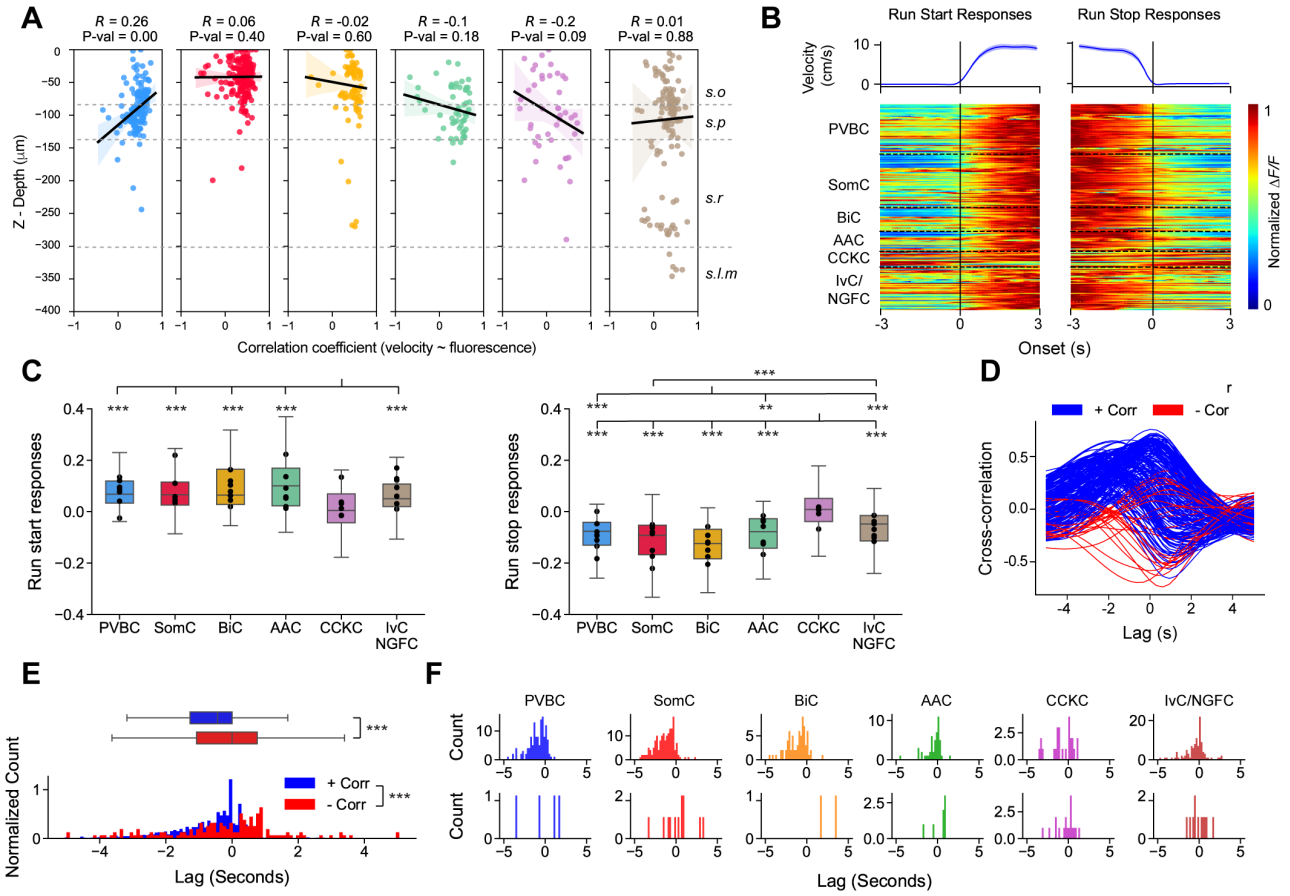


## Figure S2 - Locomotion-related activity and depth profiles (related to Figure 2)

**A**. Depth distribution as a function of correlation with velocity for each subtype. Correlation coefficient (R values) and P-values are reported for the two variables. Shaded area represents bootstrapped confidence intervals.
**B**. Top: Average velocity profile centered around run initiation (run start) and stop (run stop) events. Bottom: heatmap of activity profiles for each subtype during run start and run stop events. Each row represents the normalized activity of one neuron.
**C**. Left: Quantification of run start events. One-way ANOVA ($p < 10\text{-}5$) with post hoc Tukey's range test corrected for multiple testing (PVBC: 0.08 ± 0.08, SomC: 0.08 ± 0.11, BiC: 0.09 ± 0.15, AAC: 0.12 ± 0.13, CCKC: -0.005 ± 0.13, IvC/NGFC: 0.062 ± 0.11, median ± IQR). Right: quantification of run stop events. One-way ANOVA ($p < 10\text{-}10$) with post hoc Tukey's range test corrected for multiple testing (PVBC: -0.09 ± 0.11, SomC: -0.12 ± 0.15, BiC: -0.164 ± 0.19, AAC: -0.111 ± 0.14, CCKC: 0.03 ± 0.16, IvC/NGFC: 0.06 ± 0.09, median ± IQR). Mouse averages are indicated by the black dots.
**D**. Representative cross-correlation traces between ΔF/F signals and animal's velocity. Each line represents one cell, color-coded by its positive (blue) or negative (red) correlation with velocity.
**E**. Distribution of lags for all positively (n = 1429; median ± IQR: -0.44 ± 1.27) and negatively (n = 156; median ± IQR: 0 ± 1.8) correlated INs, regardless of subtype (n = 7 mice). Two-sample Kolmogorov-Smirnov test on distributions ($p < 10\text{-}5$). Mann-Whitney U test on populations ($p < 10\text{-}5$).
**F**. Distribution of lags per subtype for (top row) positively and (bottom row) negatively correlated cells (n = 134 PVBC, 180 SomC, 75 BiC, 56 AAC, 44 CCKC, 119 IvC/NGFC from 7 mice).
*p<0.05, **p<0.01, ***p<0.001.

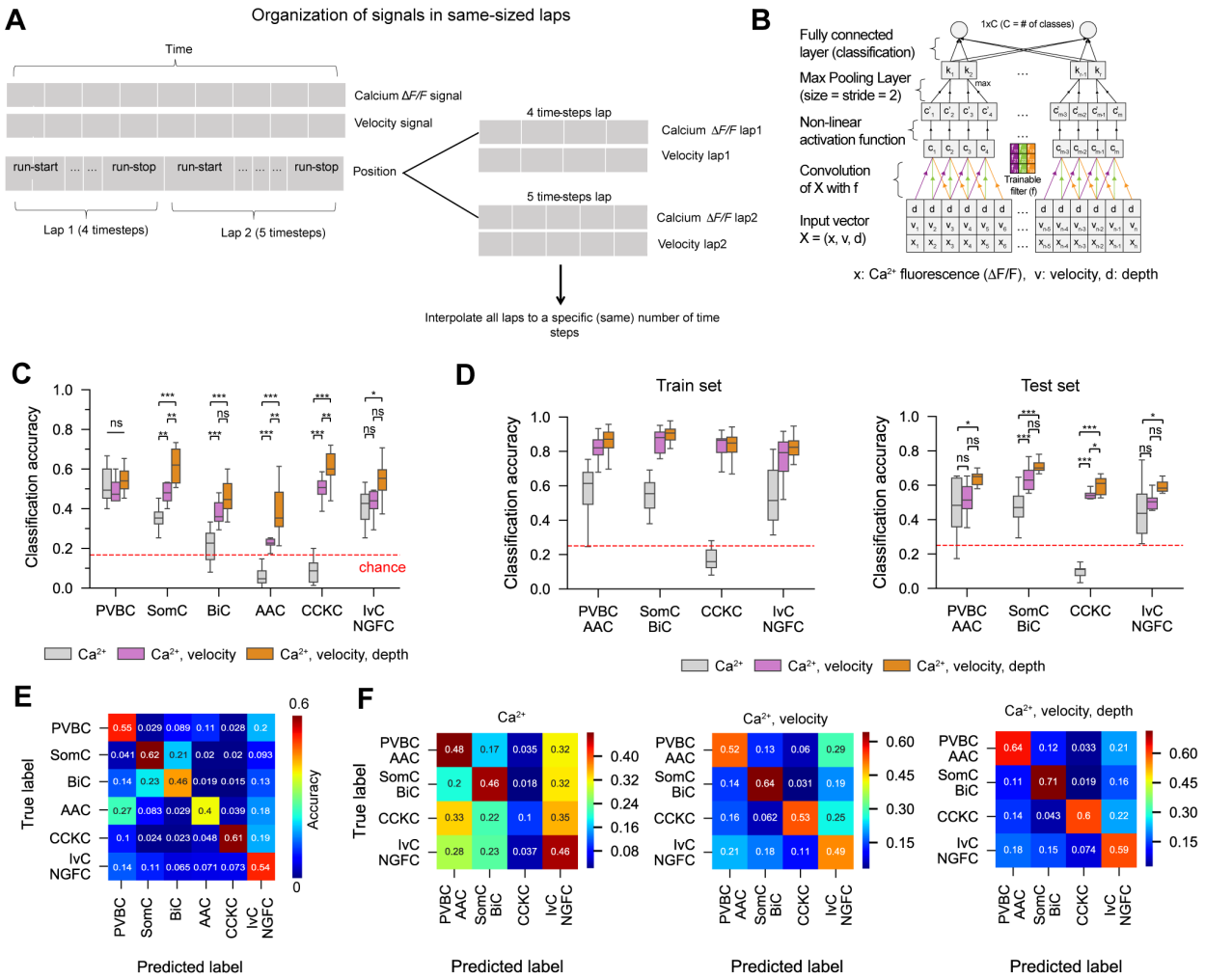


## Figure S3 - Machine Learning-based decoding of major IN subtypes (related to Figure 2)

**A**. Preprocessing flowchart for signal alignment and organization into laps. Both calcium ΔF/F and velocity signals are first broken down into laps, based on the run-start and run-stop information for each session. As signals often differ in length for the various laps/-sessions, they are interpolated to a common number of data points (length).

**B**.Proposed deep learning architecture (2D-CNN) for IN subtype decoding: The input vector X is convolved (stride=1) with a trainable filter f resulting in a vector c, to which a non-linear activation function is applied, resulting in another vector c' with the same size. A max pooling layer of size 2 is also applied to c' in order to down-sample the input representation, reducing its dimensionality. The number of the output neurons C equals to the number of classes (6 in this case).

**C**.Classification accuracy achieved by the 1D-CNN (calcium only: grey) and 2D-CNNs (calcium, velocity: purple) or (calcium, velocity, depth: orange) architectures. Prediction accuracy is measured as the percentage of correctly predicted examples for each of the cell classes, using a blind test set. Each boxplot depicts the performance obtained over 10 random splits of the data between Training and Test sets. The sizes of the Training and Test sets were the following: n = 2128 PVBC, 2128 SomC, 1928 BiC, 1248 AAC, 1128 CCKC, 2628 IvC/NGFC in the Training set and n= 75 cells for each type in the Test set. Performance in each type was compared using repeated measures ANOVA (PVBC: $p = 0.16$, SomC: $p < 0.001$, BiC: $p < 0.001$, AAC: $p < 0.001$, CCKC: $p < 0.001$, IvC/NGFC: $p = 0.037$) with post hoc Tukey's range test corrected for multiple testing.

**D**.Left: Decoding performance measured as prediction accuracy for the Training set, by the 1D-CNN (calcium only: grey) and 2D-CNNs (calcium, velocity: purple) or (calcium, velocity, depth: orange) architectures. Each box-plot depicts the performance obtained over 10 random splits of the data. The Training set consisted of n= 2052 PVBC/AAC, 2052 SomC/BiC, 1053 CCKC, 2552 IvC/NGFC training examples. Right: Same, with decoding performance measured on the Test set, consisting of 150 examples for each of the 4 classes (75 examples from each cell type of the mixed categories). Median values are reported in (D).

**E**. Confusion matrix for the 2D-CNN that was trained and tested using the calcium, velocity and depth information, as shown in panel C (orange). Rows represent the true subtypes and columns the subtypes predicted by the 2D-CNN. Many decoding errors resulted from misclassification between PV-expressing INs (PVBCs and AACs) and between SOM-expressing INs (SomCs and BiCs). For example, 27% of the AAC were misclassified as PVBC. The opposite was less pronounced (just 11% of PVBC were predicted to be AAC), possibly because the number of training examples was higher for PVBC compared to AAC, thus enabling better learning for this class.

**F**. Confusion matrices for the CNN classifiers when implementing different features: calcium only; calcium and velocity or calcium, velocity and depth. *p<0.05, **p<0.01, ***p<0.001.

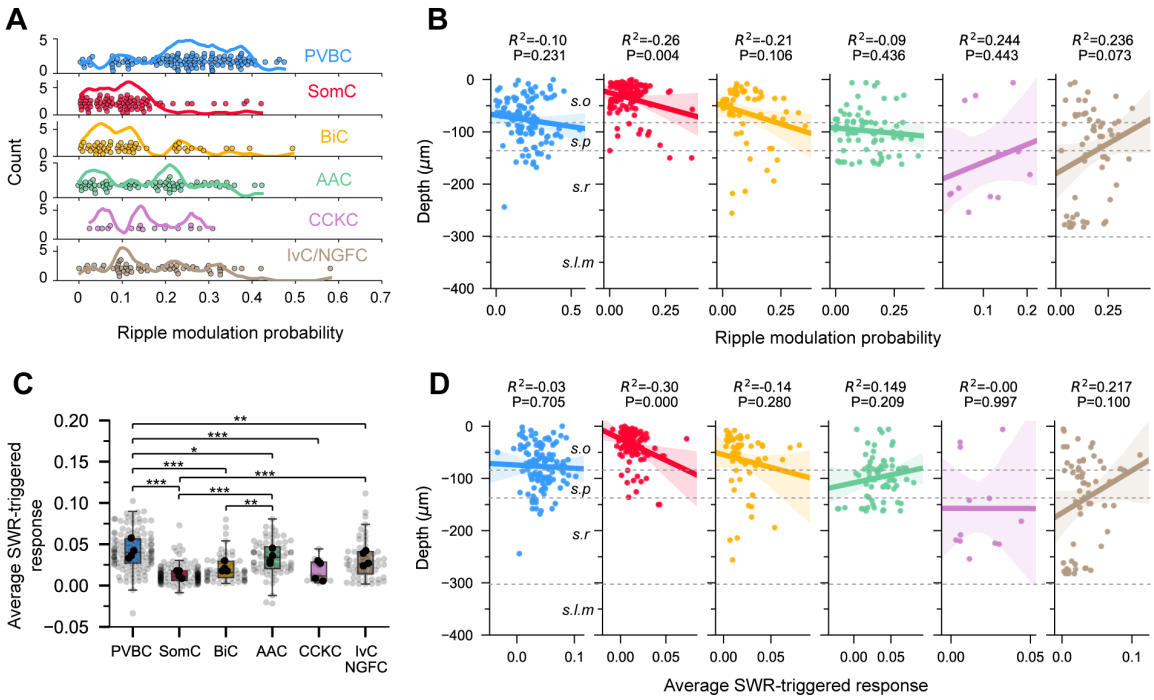


## Figure S4 - Sharp-wave ripple modulation and depth profiles (related to Figure 3)

**A**. Histogram of ripple modulation for each subtype with overlaid density kernel (same data and n as Figure 3).

**B**. Depth distribution as a function of ripple modulation for each subtype. Correlation coefficient (R values) and P-values are reported for the two variables. Shaded area represents bootstrapped confidence intervals.

**C**. Distribution of average response (n = 122 PVBC, 79 SomC, 54 BiC, 72 AAC, 16 CCKC, 58 IvC/NGFC from n = 4 mice) also showing bimodal distributions for BiC and AAC (PVBC: 0.04 ± 0.03, SomC: 0.011 ± 0.01, BiC: 0.016 ± 0.02, AAC: 0.034 ± 0.026, CCKC: 0.012 ± 0.023, IvC/NGFC: 0.026 ± 0.027, median ± IQR). One-way ANOVA ($p < 0.001$) with post hoc Tukey's range test corrected for multiple testing. Mouse averages are indicated by the black dots.

**D**. Depth distribution as a function of average response for each subtype. Correlation coefficient (R values) and P-values are reported for the two variables. Shaded area represents bootstrapped confidence intervals. *p<0.05, **p<0.01, ***p<0.001.

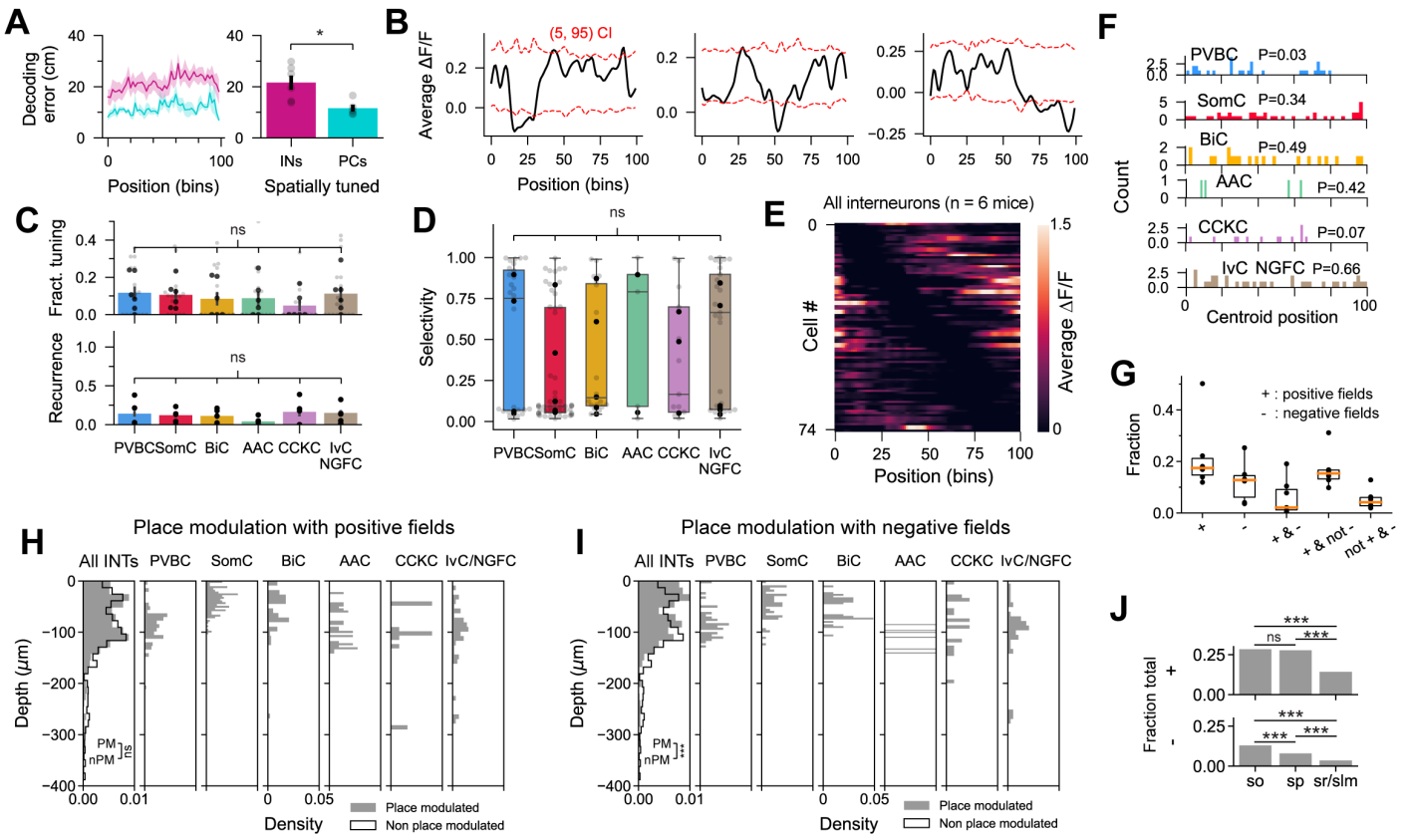


## Figure S5 - Spatially modulated interneurons with negative field (related to Figure 4)

**A**.Left: Decoding error as a function of position for spatially modulated interneurons (n = 6 mice, 21.6 ± 2.76 cm, mean ± SEM) and pyramidal place cells (n = 5 mice, 11.6 ± 0.01cm, mean ± SEM). Right: average decoding error for each group, unpaired t-test (p = 0.012). Data are represented as mean ± SEM.

**B**. Representative examples of spatially modulated interneurons with a negative field (trough). Red dashed lines represent the 5% and 95% confidence intervals of the shuffled data.

**C**. Top: Fraction of spatially modulated neurons for each subtype. Light gray dots represent sessions (n = 18 sessions from 6 mice, PVBC: 12 ± 3%, SomC: 11 ± 3%, BiC: 8 ± 3%, AAC: 9 ± 3%, CCKC: 5 ± 2%, IvC/NGFC: 11 ± 3%, mean ± SEM) and black dots represent mouse averages (one-way ANOVA, p = 0.16). Bottom: Recurrence probability (PVBC: 14 ± 2%, SomC: 12 ± 1%, BiC: 11 ± 2%, AAC: 4 ± 2%, CCKC: 16 ± 4%, IvC/NGFC: 15 ± 2%, mean ± SEM) of spatial modulation (one-way ANOVA, p = 0.64). N = 37 PVBC, 43 SomC, 20 BiC, 5 AAC, 15 CCKC, 41 IvC/NGFC from n = 6 mice. Top, bottom, data are represented as mean ± SEM.

**D**. Selectivity index (PVBC: 0.74 ± 0.85, SomC: 0.09 ± 0.64, BiC: 0.14 ± 0.74, AAC: 0.79 ± 0.8, CCKC: 0.17 ± 0.64, IvC/NGFC: 0.66 ± 0.8, median ± IQR) depicting sharpness of the tuning curve (one-way ANOVA, p = 0.35). Each dot represents one neuron's selectivity index or its average over multiple sessions if detected multiple times (n = 29 PVBC, 41 SomC, 20 BiC, 4 AAC, 13 CCKC, 32 IvC/NGFC from n = 6 mice).

**E**. Activity of 74 spatially modulated interneurons with negative field recorded in 6 mice. Each row is color coded to represent one interneuron's average ΔF/F.

**F**. Distribution of the inverse activity's centroid along the belt. P-values correspond to a Kolmogorov-Smirnov uniformity test (same n as in D).

**G**. Fraction of spatially modulated interneurons, regardless of subtype identity. "+" represents the neurons with a positive place field, "-" represents those with a negative place field. Overall, 17.4 ± 6.4% had positive fields, 12.7 ± 8.3% had negative fields, 2.1 ± 7.8% had both a positive and negative field, 15.3 ± 3.4% had strictly a positive field and no negative field, 4.2 ± 3.2% had strictly a negative field and no positive field (median ± IQR, n = 6 mice). Mouse averages are indicated by the black dots.

**H**. Depth distribution of place modulated with a positive field (filled gray, n = 1135 cells), and non-place modulated (black step, n = 3224) for all interneurons and different subtypes. Two-sample Kolmogorov-Smirnov test on distributions (p = 0.32).

**I.** Same analysis as in (H) for negative place fields. Place modulated interneurons (n = 430, non modulated n = 3929) tended to be in deeper CA1, around s.o (place modulated: -67 ± 70μm, non-place modulated: -97 ± 77μm, median ± IQR). Two-sample Kolmogorov-Smirnov test on distributions (p p < 10-5), Mann-Whitney U-test on populations (p < 10-5).

**J.** Fraction of detected place interneuron with positive (+) and negative (-) peaks, blind of subtype and pooled by layer (positive in so: 28.4%, sp: 27.6%, sr: 14.2%, negative in so: 12.9%, sp: 7.9%, sr: 3.5%, same n as in H and I). Chi-squared proportion tests. *p<0.05, **p<0.01, ***p<0.001.

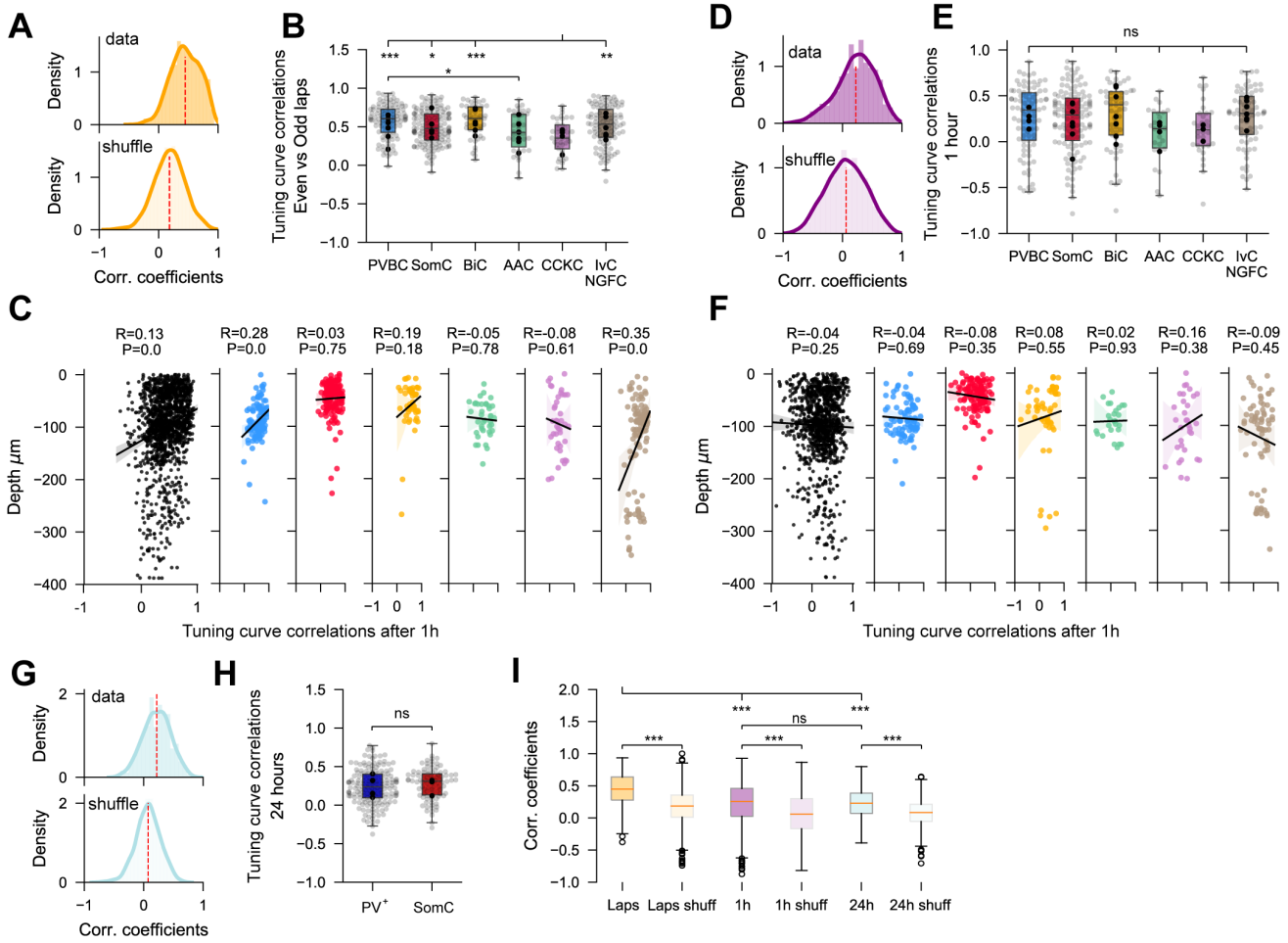


## Figure S6 – Context representation drifts rapidly within one day (related to Figure 4 and 5)

**A**. Distribution of tuning curve correlation coefficients between odd and even laps within the same session for all interneurons and shuffled data (top, bottom, n = 1430 from 6 mice).
**B**. Correlation coefficients between odd and even laps for molecularly-identified subtypes. One-way ANOVA ($p < 0.001$) with post hoc Tukey's range test corrected for multiple testing (n = 105 PVBC, 145 SomC, 50 BiC, 39 AAC, 41 CCKC, 111 IvC/NGFC from n = 6 mice).
**C**. Depth distribution for all interneurons (black) and different subtypes as a function of the correlation coefficient between the tuning curve in odd and even laps.

**D**. Distribution of tuning curve correlation coefficients between 2 sessions separated by 1 hour for all interneurons and shuffle data (top, bottom, n = 1160 from 6 mice).
**E**. Correlation coefficients between 1-hour apart sessions by molecularly-identified subtypes. One-way ANOVA ($p = 0.10$) with post hoc Tukey's range test corrected for multiple testing (n = 93 PVBC, 125 SomC, 53 BiC, 27 AAC, 34 CCKC, 82 IvC/NGFC from n = 6 mice).
**F**. Depth distribution for all interneurons (black) and different subtypes as a function of the correlation coefficient between the tuning curve between sessions separated by 1 hour.

**G**. Distribution of tuning curve correlation coefficients between 2 sessions separated by 24 hours for all interneurons and shuffle data (top, bottom, n = 643 from 4 mice).

**H**. Correlation coefficients between 24-hour apart sessions for PV+ (n = 163) and SomC (n = 93) neurons (unpaired t-test, $p = 0.17$). Data from n = 4 mice. Due to the low number of interneurons that were tracked for 24h, data for PV+ cells were pooled with mice without SATB1 staining (see Assignment of subtype identity section in Methods).

**I**. Summary statistics for (A), (C) and (E). All distributions are compared to their corresponding shuffled distribution (unpaired t-tests). Spatial tuning after 1 hour is as correlated as after 24 hours, and both are significantly lower than within session correlations. One-way ANOVA ($p < 10^{-10}$) with post hoc Tukey's range test corrected for multiple testing.

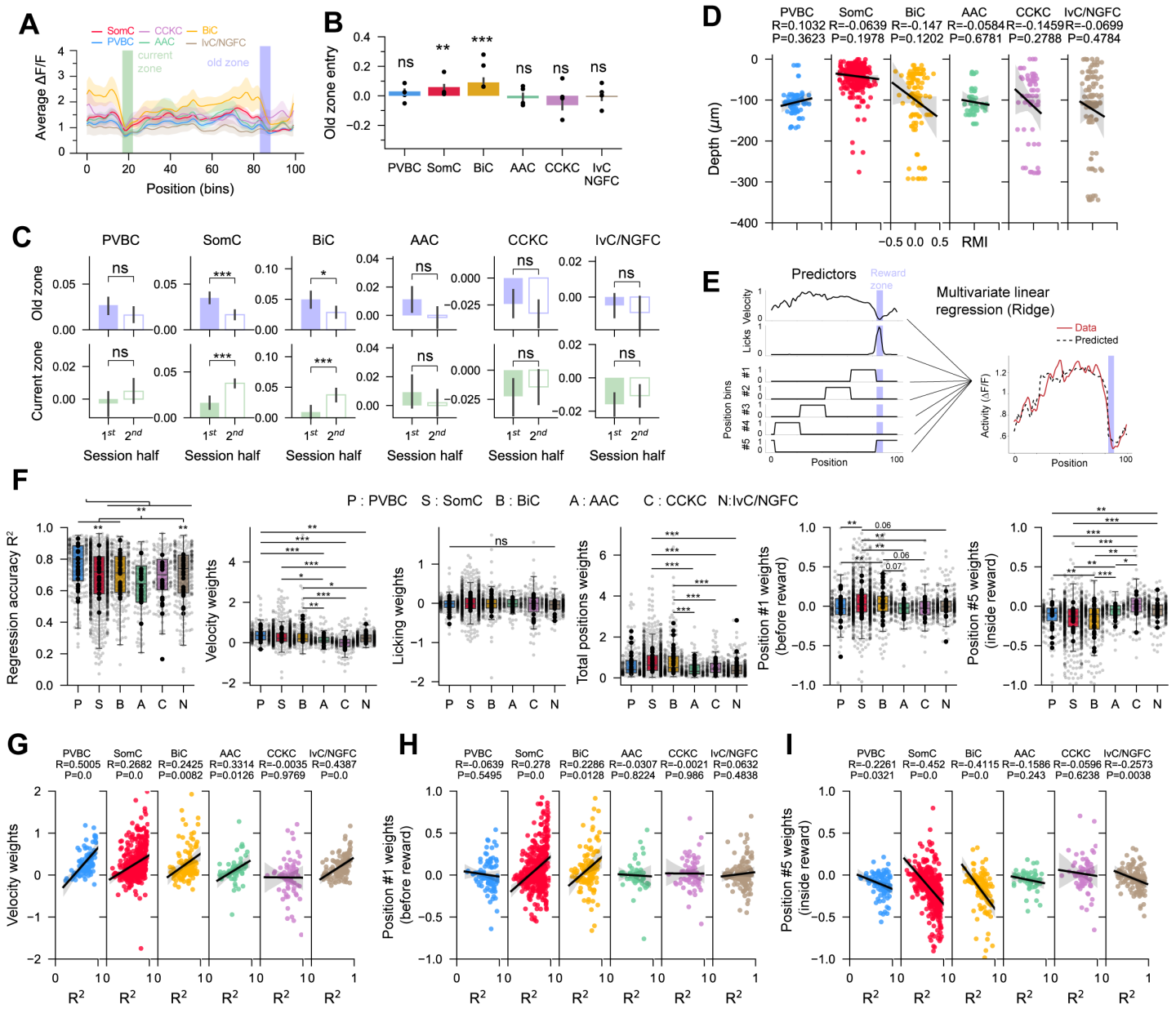


## Figure S7 - Traces of old reward zone representation in the goal-oriented learning task and multivariate regression model (related to Figure 6)

**A**. Representative average tuning curve for each subtype. BiCs and SomCs show increased activity preceding the old reward zone (blue shaded area).
**B**. Quantification of the old zone (PVBC: 0.03 ± 0.02, SomC: 0.05 ± 0.01, BiC: 0.09 ± 0.03, AAC: -0.02 ± 0.03, CCKC: -0.06 ± 0.03, IvC/NGFC: -0.01 ± 0.02, mean ± SEM) entry shows significantly higher modulation than expected by chance (one-sample t-test). N = 60 PVBC, 314 SomC, 103 BiC, 42 AAC, 38 CCKC, 78 IvC/NGFC from 4 mice.
**C.** Quantification of old zone modulation and comparison between the first half and second half of the session. The modulation in the old zone for both BiC and SomC decreases with time while the modulation in the current reward zone increases, showing that BiC and SomC have remnants of the old reward representation. Values for Old zone (average first zone and second zone ± SEM, p-value for paired t-test); PVBC: 0.027 and 0.016 ± 0.009, p = 0.14; SomC: 0.035 and 0.017 ± 0.006, p = 0; BiC: 0.05 and 0.028 ± 0.013, p = 0.041; AAC: 0.011 and -0.001 ± 0.009, p = 0.08, CCKC: -0.024 and -0.033 ± 0.013, p = 0.52; IvC/NGFC: -0.005 and -0.009 ± 0.007, p = 0.63). Values for Current zone (average first zone and second zone ± SEM, p-value for paired t-test); PVBC: -0.003 and 0.005 ± 0.007, p = 0.13; SomC: 0.016 and 0.038 ± 0.007, p = 0; BiC: 0.009 and 0.037 ± 0.01, p = 0; AAC: 0.009 and 0.002 ± 0.011, p = 0.98; CCKC: -0.022 and -0.014 ± 0.015, p = 0.46; IvC/NGFC: -0.016 and 0.011 ± 0.007, p = 0.35).
**D**. Depth distribution as a function of the Reward Modulation Index (see Figure 6) for the different subtypes.
**E.** Schematic of the multivariate linear Ridge regression to disentangle the effects of various behavioral variables on interneuron activity. We used 7 variables: the velocity, licking, and positions (binned into 5 segments) to fit to the calcium signal.
**F.** Results of the regression. PVBC and AAC were respectively the best and the least well fitted subtypes (highest and lowest $R^2$). The coefficient (weight) for velocity predictor was higher for PVBC, SomC and BiC, meaning that velocity has a higher impact on the regression of the calcium signal, consistent with results in Figure 2. Licking had a low contribution, consistent across all subtypes. The total position weights (sum of all 5 segments) was higher for SomC and BiC. As expected, the segment before the reward zone has a stronger weight for SomC and BiC, while the segment inside the reward zone was increased in CCKC, IvC and decreased in PVBC, SomC and BiC (strong negative weights in those 3 subtypes)
**G**. Correlation between the velocity weights and $R^2$, confirming that neurons more modulated by speed were more accurately fitted. CCKC did not show such trend, confirming that velocity has no impact on the calcium signal of these cells.
**H.** Correlation between the weights of position segment #1 and $R^2$. For SomC and BiC, the increased calcium activity before the reward zone was captured by this segment, which explains that the fit was more accurate in a subset of these neurons. Such correlation is absent in all other subtypes because they do not present such increase (see Figure 6).
**I.** Inversely, for the position segment inside the reward zone, strong negative weights meant better fit for most subtypes. *p<0.05, **p<0.01, ***p<0.001.